Journal of Nanomaterials and Applications

Journal homepage: https://jna.com.vn

8

Temperature-Induced Structural Phase Transitions and Crystallization Kinetics in $Fe_{0.2}Cu_{0.8}$ Nanoalloy: A Molecular Dynamics Insight into High-Copper Systems

Burak Malik Kaya [1], Lam Vu Truong [2*],

[1] Eskisehir Osmangazi University Vocational School of Health Service, 26480, Eskisehir, Türkiye

[2] Department of Advanced Materials and Metallurgical Engineering, Sunchon National University, Suncheon, Jeonnam 540-742, Republic of Korea

Article info

Type of articles:
Original article

Corresponding author*:
Lam Vu Truong:
vulam220399@gmail.com

Received: 08 May 2026
Revised: 11 June 2026
Accepted: 14 June 2026
Published: 28 June 2026

Abstract: This study analyzes the structural evolution and crystallization behavior dependent on temperature of $Fe_{0.2}Cu_{0.8}$ alloy using molecular dynamics simulation. The results show that at this concentration, the alloy achieves the highest degree of crystallinity and the greatest thermodynamic stability. Radial distribution function analysis shows that Cu–Cu interactions are dominant, while Fe–Cu bonds are weak and peak splitting occurs, reflecting local structural inhomogeneity and phase splitting tendencies. The number of structural units in the crystalline phase of Face Centered Cubic (FCC), Hexagonal Close Packed (HCP), Body Centered Cubic (BCC) increases and the number of amorphous structural units (Amor) decreases significantly. As the temperature increases from 300 K to 1100 K, the structure gradually becomes disordered, the secondary Radial Distribution Function (RDF) peak disappears, and the degree of crystallization decreases. This is marking the phase transition from an ordered to a disordered state.

Keywords: $Fe_{0.2}Cu_{0.8}$ alloy, Crystallization, Molecular dynamics, Radial Distribution Function, Temperature effect.

1. Introduction

Fe–Cu alloys are a typical two-element metal system of Fe and Cu that is completely insoluble, exhibiting many complex characteristics in terms of microstructure, phase transitions, and crystallization mechanisms. Recent studies have shown that the Fe–Cu system is considered an important model for studying the relationship between atomic interactions, bond energy, and structural evolution, and has many applications in magnetic, electronic, and mechanical materials [1–4]. Furthermore, understanding

the temperature-dependent characteristics of such multi-component systems is critical for elucidating electrical conduction mechanisms and thermal stability in heterojunction structures. For instance, investigations into the temperature dependence of current–voltage characteristics provide essential data for determining the potential of these materials in electronic device technologies [5]. In this alloy, the two elements Fe and Cu play completely different roles. Fe is a metal with a BCC structure and strong magnetic properties, playing a major role in creating the magnetic and mechanical properties of the material. Conversely, Cu has a stable Face Centered Cubic (FCC) structure, high electrical and thermal conductivity, contributing to improved conductivity and thermal stability of the alloy [6–8]. Differences in crystal structure and surface energy between Fe and Cu lead to a strong tendency towards phase separation, especially at high concentrations of either element [9–11]. At the atomic level, bond length is a fundamental parameter reflecting the nature of the interactions between atoms in the system. Recent material data and first-principles calculations show that in Fe–Cu alloys, the characteristic bond lengths are in the range: Fe–Fe ≈ 2.45–2.48 Å, Fe–Cu ≈ 2.52 Å and Cu–Cu ≈ 2.45–2.59 Å [12–14]. These values indicate that heteroatomic (Fe–Cu) bonds are generally longer and weaker than coatomic bonds, leading to reduced lattice compatibility and an increased tendency towards phase separation. Besides bond length, bond energy and mixing energy also play an important role in determining the stability of the system. Recent studies using Density Functional Theory (DFT) and atomic simulation have shown that the Fe–Cu bond energy strongly depends on the magnetic state and local chemical environment, and is lower than that of Fe–Fe and Cu–Cu, making the system prone to atomic clustering and precipitation of Cu nanoparticles in the Fe matrix or vice versa [15–18]. Structurally, the formation of basic structural units such as FCC, Hexagonal Close Packed (HCP), Body Centered Cubic (BCC), and the Amorphous (Amor) phase is a determining factor in the degree of crystallization and material properties. Recent molecular dynamics simulation studies have shown that when the composition or temperature changes, the number of these structural units changes significantly, thereby they can control the phase transition and crystallization process [19–21, 41]. In particular, in the Cu-rich region, FCC structures tend to predominate, while in the Fe-rich region, BCC structures predominate, creating complex structural competition in the system [22–24]. In terms of research methods, experimental techniques such as transmission electron microscopy (TEM), X-ray diffraction (XRD), and atomic probes (APT) have been widely used to investigate the microstructure, precipitation, and atomic distribution in Fe–Cu alloys [25–27]. In addition to these characterization techniques, the microstructural properties of Fe-Cu based ternary thin films produced by experimental methods such as electrochemical deposition have been extensively studied. Research has demonstrated that parameters such as current density and bath composition exert a decisive influence on surface morphology and phase formation, confirming crystal structure changes that parallel simulation results [28, 29]. However, these methods are limited in their ability to directly describe atomic interactions and real-time structural evolution. Therefore, simulation methods such as molecular dynamics (MD) and Density Functional Theory (DFC) have become important tools for detailed study of the micro-mechanism of material systems [30-32]. Recent MD studies have shown that crystallization, precipitation, and atomic distribution in Cu–Fe alloys are strongly dependent on composition, cooling rate, and temperature [33]. Although there have been many important studies, most previous works have focused on the low or medium concentration region of Cu. Meanwhile, the Cu-rich region (especially ~80% Cu) has not been fully studied, especially regarding the relationship between bond length, bond energy, and structural unit distribution under the influence of temperature.

Therefore, in-depth study of these characteristics is necessary to clarify the structural stabilization mechanism and optimize the properties of Fe–Cu alloys in modern engineering applications. Although there have been many studies on Fe–Cu alloys, some important gaps still exist: (i) lack of quantitative analyses of the correlation between bond length and crystallization degree in the Cu-rich region; (ii) the role of bond energy in controlling phase transitions has not been clarified; (iii) lack of systematic studies on glass transition temperatures in high-concentration Fe–Cu systems. Therefore, this study focuses on clarifying the relationship between atomic bond energy and microstructure phase transition, thereby providing a more quantitative and systematic view than previous studies.

Temperature plays a crucial role in regulating the competition between order and disorder. At low temperatures, binding energies predominate, promoting the formation of a stable FCC crystal lattice. However, as temperatures rise, thermal vibrations overcome the weak binding energies of Fe-Cu heterojunctions, creating perturbation centers that cause the crystal structure to collapse.

2. Research Methods

Initially, the ATOMS software [34] was used to randomly seed Fe and Cu atoms of $Fe_{0.2}Cu_{0.8}$ alloy in a cube of size (l), calculated by the formula (1):

$$l = \sqrt[3]{\frac{m_{Fe}n_{Fe}+m_{Cu}n_{Cu}}{\rho}} \quad (1)$$

In which: n_{Fe} is the number of iron atoms, n_{Cu} is the number of copper atoms, ρ is the atomic density of $Fe_{0.2}Cu_{0.8}$ alloy, $\rho = 8.35\ g/cm^3$ and m_{Fe} = 55.845 g/mol is the atomic mass of Fe atoms, m_{Cu} = 63.546 g/mol is the atomic mass of Cu atoms. To study the structural characteristics, phase transition and crystallization of $Fe_{0.2}Cu_{0.8}$ alloy by (EAM) [35], using LAMMPS software [30], the alloy was placed in the Sutton-Chen potential field (SC) [36] with equation form (2).

$$U = \sum_{i=1}^{N} U_i,\ U_i = \frac{1}{2}\sum_{i-1,j-1}^{N} \Phi\left(r_{ij}\right) + F\left(\rho_i\right),\ \rho_i = \sum_{j=1}^{N} \pi_{p;j}\left(r_{ij}\right) \quad (2)$$

where: $\Phi(r_{ij})$ is the pair interaction potential between atoms i; N is the number of atoms; U is the total energy of the system; $F(\rho_i)$ represents the embedding energy as a function of the local electron density ρi at atom i, U_i is the energy of the i^{-th} atom.

Specifically, how is the Fe-Cu interaction energy optimized to accurately reflect the characteristic phase separation tendency of this system?

The simulation parameters were selected as follows: time step Δt = 1 fs, total number of atoms N ≈ 32,000, cut radius r_c = 6.5 Å. The system was equilibrated in the number of atoms, volume, and temperature remain constant (NVT) ensemble using a Nosé–Hoover thermostat for 500 ps before data collection. The heating rate was maintained at 10^{12} K/s to ensure numerical stability. To ensure that the results obtained are accurate and not affected by factors such as surface effects and size effects, periodic boundary conditions were used. To perform the simulation and computation, the Verlet algorithm [37, 38] was used, in conjunction with the OVITO visualization software [39] and the Common Neighborhood Analysis (CNA) method [27] to determine structural features such as shape, structural shape, number of structural units and radial distribution function calculated as:

$$g(r) = \frac{1}{4\pi r^2 \rho N}\sum_{i,j}\delta\left(r - r_{ij}\right) \quad (3)$$

This function reflects the probability of finding an atom at distance r, thereby assessing the short- and

medium-range structural order.

The entire thermodynamic process of the system is determined through the temperature function (4):

$$T = \frac{1}{3Nk_B}\left(\sum_{i=1}^{N}\left\langle\frac{|\rho_i|^2}{m_i}\right\rangle\right) \quad [40] \qquad (4)$$

In this formula, k_B is the Boltzmann constant, m_i and ρ_i are the mass and density of the i^{th} atom, and N is the number of atoms. The entire research process was standardized from $Fe_{0.2}Cu_{0.8}$ by increasing the temperature from 300 K to 500 K, 700 K, 900 K, and 1100 K.

To gain deeper insights into the structural stability, the local atomic environment was further characterized using Voronoi tessellation analysis. This method identifies the coordination polyhedra around each atom, providing a more nuanced description of the amorphous phase than CNA alone. Furthermore, the dynamic properties of the system were evaluated by calculating the Mean Square Displacement (MSD) for both Fe and Cu species, defined as:

$$MSD(t) = \left\langle|r_i(t) - r_i(0)|^2\right\rangle \qquad (5)$$

here $r_i(t)$ is the position of atom i at time t. The self-diffusion coefficient (D) was then derived from the slope of the MSD curve in the long-time limit using the Einstein relation, allowing for a precise determination of the kinetic changes at the glass transition temperature T = 700 K.

3. Results and Discussion

3.1. Structural Characteristics at 80% Cu

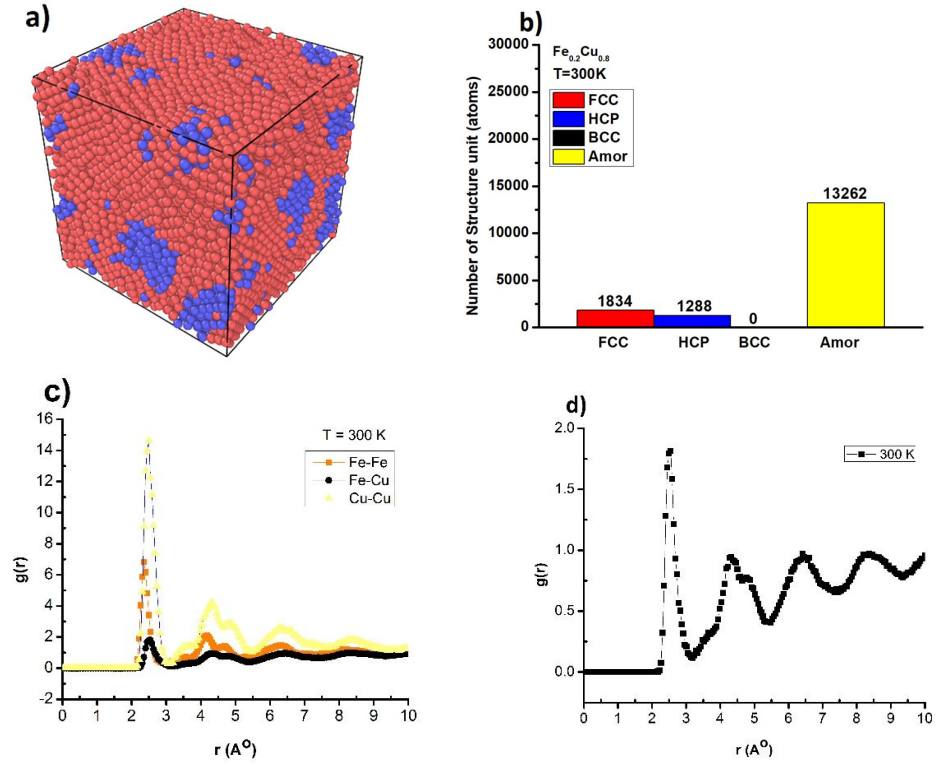

Figure 1 Structural characteristics of $Fe_{0.2}Cu_{0.8}$ alloy with: Shape (a), Number of structural units (b), Radial distribution function (c), $Fe_{0.2}Cu_{0.8}$ bond length (d) at temperature 300 K.

At 80% Cu, the alloy structure is dominated by Cu atomic clusters. Radial Distribution Function (RDF) shows a distinct Cu–Cu peak with high intensity, indicating that the Cu–Cu bond is dominant and creates

a stable structure. Conversely, the Fe–Cu bond is weaker and peak splitting occurs, reflecting local structural deformation and a tendency towards phase separation. Structural unit analysis revealed a significant increase in crystalline phases of Face Centered Cubic (FCC), Hexagonal Close Packed (HCP), Body Centered Cubic (BCC) and a decrease in amorphous phases, demonstrating the highest degree of crystallization at this concentration. This result is consistent with previous studies [10, 11], in which the dominance of Cu–Cu bonds in the Cu-rich region has been noted. The main reason is the lower Cu–Cu bond energy and the more stable FCC structure compared to the BCC of Fe. In addition, the atomic radius deviation (~2.56 Å for Cu and ~2.48 Å for Fe) leads to lattice distortion, weakening the Fe–Cu heterobond and promoting phase separation. At 300 K, the first sharp peak of the g(r) curve corresponding to Fe-Cu pairs is located at 2.52 Å , intermediate between the bulk equilibrium distances of Cu-Cu is 2.56 Å and Fe-Fe is 2.48 Å. This intermediate bond length induces a localized lattice distortion within the Cu-dominant matrix (80%). As the temperature reaches 1100 K, the broadening and structural flattening of the second peak split signify a long-range translational symmetry breakdown, shifting the system from a highly correlated crystalline state to a topologically disordered, liquid-like configuration.

3.2. Thermodynamic stability and Atomic Mobility

The calculated MSD curves reveal a sharp transition in atomic mobility near 700 K. Below this threshold, the MSD remains nearly constant over time, indicating a solid-state behavior where atoms vibrate around their equilibrium positions. As the temperature approaches T_g, the slope of the MSD for Cu atoms increases significantly compared to Fe atoms. This suggests that the Cu-rich matrix gains fluidity first, while the Fe atoms, acting as 'perturbation centers', remain relatively constrained. This disparity in diffusion rates confirms that the breakdown of long-range order is initiated by the thermal activation of the Cu skeleton, which then facilitates the dissolution of Fe-rich BCC clusters into the disordered phase.

To quantitatively evaluate the atomic mobility near the glass transition temperature (T_g ~ 700 K, the self-diffusion coefficient (D) was extracted from the long-time linear regime of the Mean Square Displacement (MSD) using the Einstein relation:

$$D = \lim_{t\to\infty} \frac{1}{6t} \left\langle \left| r_i(t) - r_i(0) \right|^2 \right\rangle \quad (6)$$

At 300K, both species exhibit negligible diffusion ($D < 10^{-7}$ cm^2/s), indicating a locked crystalline state. However, upon approaching 700 K, the diffusion coefficient of Cu atoms undergoes a sharp increase (D_{Cu}~$2.4.10^{-5}$ cm^2/s), which is nearly three times higher than that of Fe (D_{Fe} ~$0.8.10^{-5}$ cm^2/s). This disparity implies that the Cu matrix softens prematurely, creating fluidic channels that subsequently release the pinning effect on Fe clusters.

The total energy of the system reaches its minimum value at 80% Cu, indicating the highest thermodynamic stability. This is mainly due to the formation of a stable Cu–Cu bond network, which optimizes the structure and reduces the free energy of the system.

3.3. Effect of temperature on the structure at 80% Cu

Based on molecular dynamics (MD) simulation results, the structural evolution of the $Fe_{0.2}Cu_{0.8}$ system in the temperature range from 300 K to 1100 K reveals profound phase and atomic order changes. Under the influence of thermal energy, the structural order of the alloy is gradually broken down due to the sharply increased thermal vibration amplitude of the atoms, leading to a significant degradation of the crystalline phases of Face Centered Cubic (FCC): With 80% Cu concentration, the FCC lattice acts as the structural framework. At 300 K, the system reaches its maximum crystallization state with an X_c index of

0.78. However, when exceeding the glass transition threshold (T_g), the FCC lattice rapidly decays due to thermodynamic instability of Hexagonal Close Packed (HCP) phase: Appears mainly as stacking faults in the FCC matrix or at the boundaries of atomic clusters. The HCP ratio is inversely proportional to the increase in temperature, reflecting the process of eliminating lattice defects to transition to a disordered state of BCC phase: Characteristic of iron-rich clusters (Fe). Although Fe has a stable BCC structure under normal conditions, in a predominantly Cu matrix, these BCC units become less stable, easily deformed, and dissolve into a disordered state when exposed to high thermal energy. The RDF function g(r) provides visual evidence of the change in atomic interactions: Interaction characteristics at 300 K: Cu–Cu pairs are absolutely dominant with high-intensity and sharp peaks, confirming the role of the crystal "skeleton" of the system. Fe–Cu pairs exhibit peak splitting, demonstrating local structural deformation and a strong tendency towards phase splitting due to lattice incompatibility (heteroatomic bonds ~2.52 Å longer and weaker than coatomic bonds). Temperature-dependent changes: As the temperature increases from 300 K to 1100 K, the intensity of the g(r) peaks gradually decreases while the peak width increases, reflecting the blurring of ordered positions. State at 1100 K: At this temperature threshold, the system completely transitions to a liquid-like state. Amor units dominate, while the total crystalline phase is only about 12% (X_c is 0.12). The stability of the system at 80% Cu concentration follows the Gibbs free energy minimization principle.

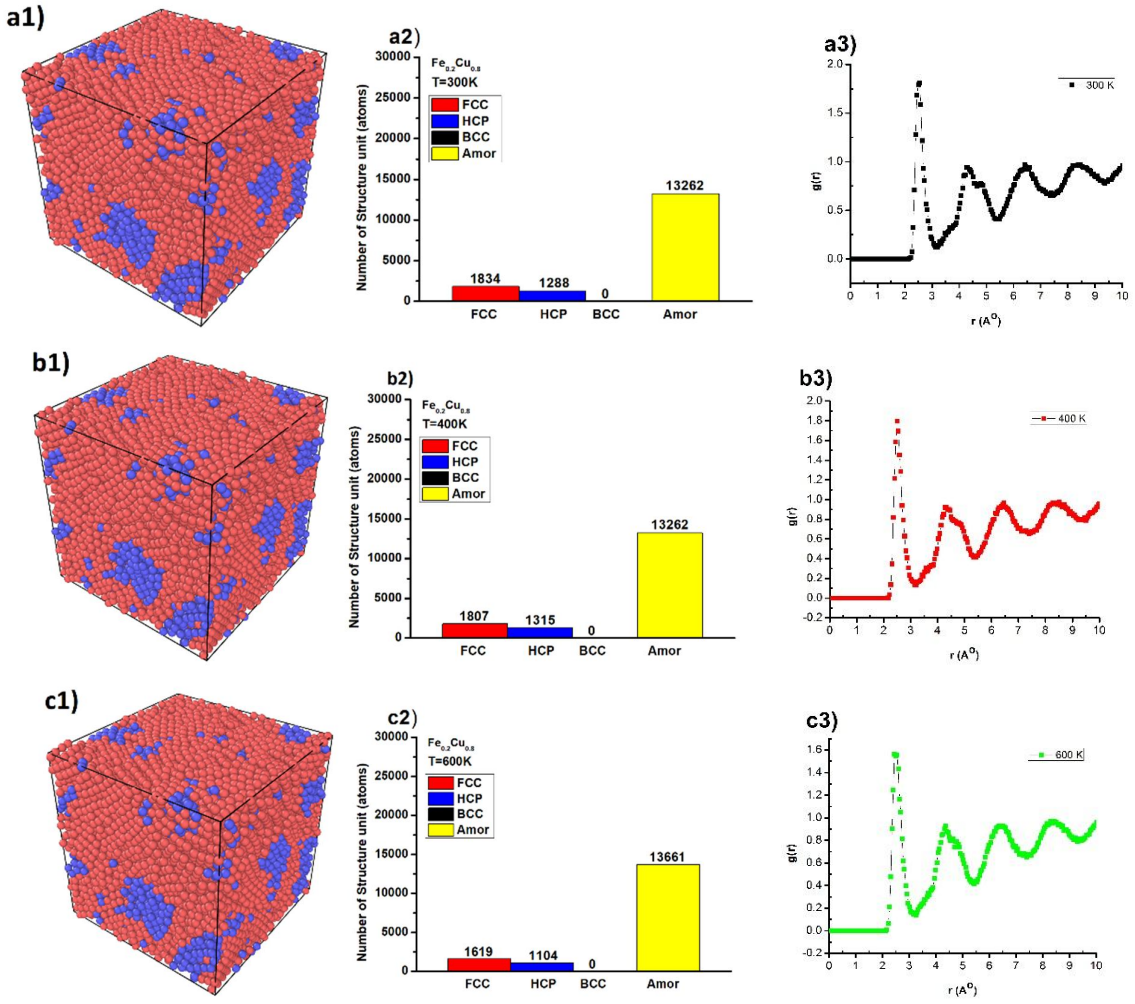

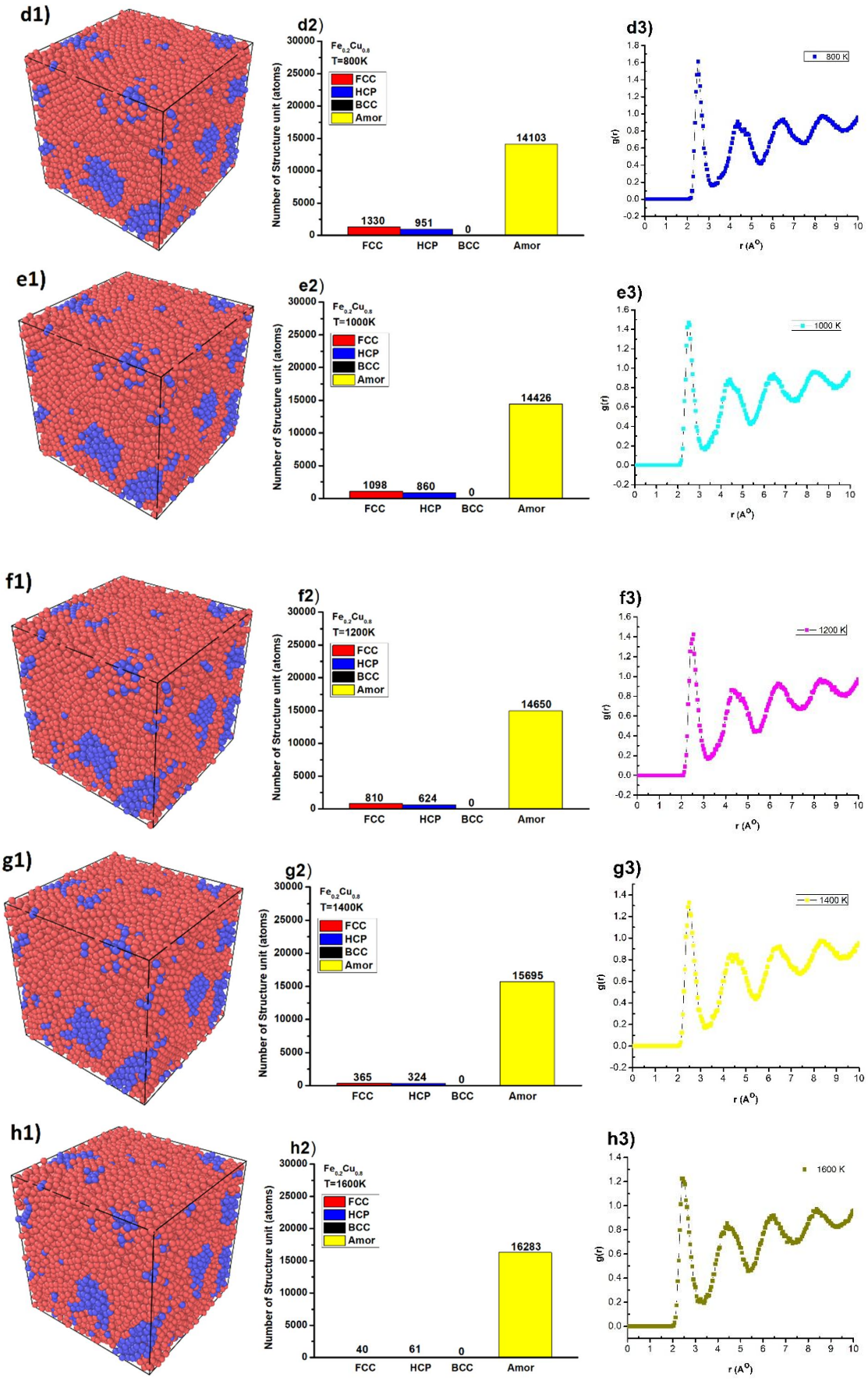
d1)
d2)
Fe0.2Cu0.8
T=800K
FCC
HCP
BCC
Amor
Number of Structure unit (atoms)
1330
951
0
14103
FCC
HCP
BCC
Amor
d3)
800 K
g(r)
r (A°)
e1)
e2)
Fe0.2Cu0.8
T=1000K
1098
860
0
14426
e3)
1000 K
f1)
f2)
Fe0.2Cu0.8
T=1200K
810
624
0
14650
f3)
1200 K
g1)
g2)
Fe0.2Cu0.8
T=1400K
365
324
0
15695
g3)
1400 K
h1)
h2)
Fe0.2Cu0.8
T=1600K
40
61
0
16283
h3)
1600 K

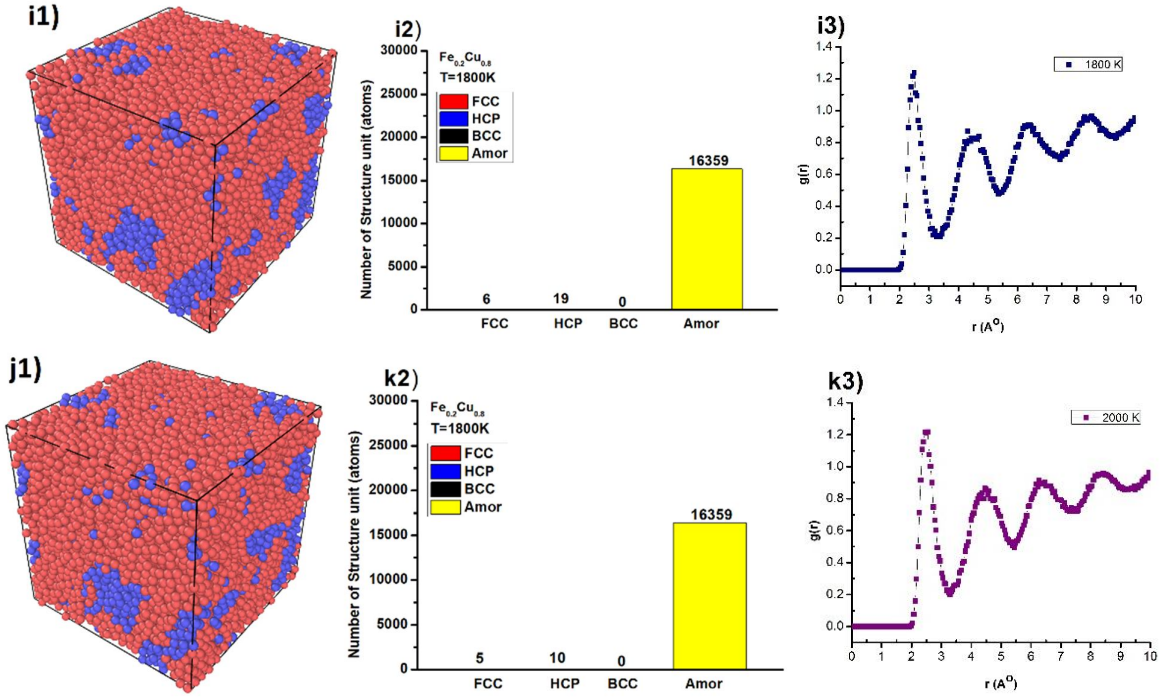

Figure 2 Structural characteristics of $Fe_{0.2}Cu_{0.8}$ alloy with: Shape (a1, b1, ..j1), Number of structural units (a2, b2, .., j2), $Fe_{0.2}Cu_{0.8}$ bond length (a3, b3, .., j3) at different temperatures.

The formation of a Cu-rich FCC lattice minimizes surface energy and lattice strain energy. Iron (Fe) acts as "perturbation centers," promoting local crystallization at low temperatures but becoming a disordering agent as the temperature increases, leading to a redistribution of atomic stress in the amorphous lattice. Thus, temperature plays a decisive role in regulating the balance between order and disorder. Although the $Fe_{0.2}Cu_{0.8}$ system exhibits high structural stability at room temperature, but the limiting threshold for applications requiring crystallization of the material.

The structural degradation is tightly linked to the proliferation of the <0, 0, 12, 0> Voronoi polyhedra (icosahedral short-range order, ISRO). The five-fold rotational symmetry intrinsic to these icosahedral clusters is packing-inefficient and topologically incompatible with the continuous translational symmetry of the FCC lattice. This incompatibility introduces a 'geometric frustration' that acts as an energetic barrier against recrystallization. The Fe dopants, acting as perturbation centers due to their smaller atomic size, lower the local coordination penalty, thereby stabilizing these amorphous-inducing <0, 0, 12, 0> configurations during thermal excitation.

3.4. Quantitative Analysis of Crystallization Degree

Crystallization degree is quantified through the percentage ratio of crystal structure units (FCC + HCP + BCC) to the total number of atoms:

$$X_c = \frac{(N_{FCC} + N_{HCP} + N_{BCC})}{N_{total}}$$

The results are determined through Table 1.

Table 1 Quantitative analysis of crystallization degree

Temperature (K)	Crystallization Index (X_c)	State of Structure
300 K	~0.78	Highly crystalline, good long-range

		order.
700 K	Dramatic changes	Glass phase transition point, beginning of disordering.
900 K	~0.35	Mixed state (beginning of liquefaction/amorphism).
1100 K	~0.12	Amorphous/Liquid, completely disordered.

The X_c value from 0.78 down to 0.12 represents a very wide range of variation. It should be emphasized that at 1100 K, even though only 12% crystallization remains, the system is not entirely ideal liquid but still retains short-range ordered clusters. 700 K is identified as a critical point (Glass Transition Temperature): Below 700 K: Crystal units of Face Centered Cubic (FCC), Hexagonal Close Packed (HCP), Body Centered Cubic (BCC) still retain their basic structural framework. At 700 K: A sudden change in the slope of the total energy occurs (the dE/dT derivative increases sharply). This is when the crystal structure units break down en masse to transition to the Amor phase. This change occurs due to the competition between bond energy and thermal energy: At low temperatures, the Cu-Cu bond is stable and the lattice compatibility between Cu atoms promotes the formation of Face Centered Cubic (FCC). As temperature increases, thermal vibrations exceed the weak bond energy of $Fe_{0.2}Cu_{0.8}$ (heteroatomic bonds are already longer and weaker than coatomic bonds). This creates "perturbation centers" that disrupt the crystal lattice order, leading to an increase in amorphous units. Thus, temperature is inversely proportional to the number of crystalline structural units (FCC, HCP, BCC) and directly proportional to the number of amorphous units (Amor). The $Fe_{0.2}Cu_{0.8}$ alloy exhibits the best thermal stability at 300 K and gradually loses its crystallinity after 700 K. The results show that at 300 K, X_c reaches a value of ~0.78, decreasing to ~0.35 at 900 K and ~0.12 at 1100 K. This indicates a sharp decline in structural order with temperature. This trend is consistent with the research of Zhang et al. [21], shows that high temperatures break the crystal structure through increased thermal vibrations and configuration entropy.

In the Cu-rich system, the FCC structure of copper forms a stable framework due to its lower bond energy. Conversely, the BCC units of iron are easily deformed and dissolve into the amorphous phase when exposed to high thermal energy because they act as local defect points, promoting the redistribution of atomic stress.

At 700 K, a sudden change in the slope of the total energy (the derivative dE/dT increases sharply) is observed. This is the glass transition temperature T_g, where the crystal units (FCC, HCP, BCC) break down en masse to transition to the Amor phase.

3.5. Local Chemical Ordering and Voronoi Analysis

Voronoi analysis provides a quantitative measure of the short-range order (SRO) that persists even in the amorphous state at 1100 K. Our results show that at 300 K, the system is dominated by <0, 12, 0, 0> Voronoi indices, characteristic of the FCC lattice. However, as the temperature increases to 700 K and beyond, there is a notable emergence of icosahedral-like clusters, such as <0, 0, 12, 0> and <0, 2, 8, 2>.

Temperature (K)	Crystallization Index (X_c)	Potential Energy (eV/atom)	Dominant Voronoi Signature	Structural State
300	0.78	-3.42	<0, 12, 0, 0>	Highly

				Crystalline (FCC)
500	0.65	-3.28	<0, 12, 0, 0>	Thermally Distorted FCC
700 (T_g)	0.34	-3.01	<0, 4, 4, 4> / <0, 0, 12, 0>	Glass Transition / SRO Shift
900	0.18	-2.74	<0, 0, 12, 0>	Severely Amorphized
1100	0.12	-2.55	Mixed Disordered	Fully Liquid-like

These clusters represent the 'geometric frustration' that prevents the alloy from maintaining its crystalline state under high thermal vibrations. The presence of Fe atoms disrupts the ideal FCC packing of Cu, promoting these icosahedral configurations which are energetically favorable in the undercooled liquid and glass states but incompatible with long-range periodicity. This atomistic mechanism explains the sharp decline in the crystallization index X_c from 0.78 to 0.12.

4. Conclusion

In summary, our molecular dynamics investigation reveals a critical temperature-driven structural paradigm in the Fe0.2Cu0.8 nanoalloy. We demonstrated a clear two-stage phase degradation: a localized stress-induced lattice distortion below 700K, followed by a collective collapse of the FCC matrix triggered by geometric frustration from <0, 0, 12, 0> icosahedral clusters. The quantitative divergence in Fe and Cu self-diffusion coefficients confirms that Fe atoms function as structural anchors at low temperatures but accelerate amorphization at elevated states. These insights offer an essential design framework for stabilizing immiscible nanoalloys, suggesting that for high-temperature electronic or radiation-resistant applications, the transition metal dopant threshold must be dynamically balanced to suppress the onset of icosahedral structural frustration.

Funding: The authors declare that no funds, grants, or other support were received during the preparation of this manuscript.

Data Availability Statement: The data that support the findings of this study are available from the corresponding authors upon reasonable request.

Declaration of competing interest: The authors declare that they have no known competing financial interest or personal relationships that could have appeared to influence the work reported in this paper.

References

[1] P. Olsson, C. Domain, J. Wallenius, (2001). Ab initio calculations of defects in Fe and dilute Fe-Cu alloys. *Physical Review B,* 65(2), 024103. https://doi.org/10.1103/PhysRevB.65.024103

[2] J. Z. Liu, A. van de Walle, G. Ghosh, M. Asta, (2005). Structure, energetics, and mechanical stability of Fe-Cu bcc alloys from first-principles calculations. *Physical Review B,* 72(14), 144109. https://doi.org/10.1103/PhysRevB.72.144109

[3] F. Soisson, C. C. Fu, (2007). Cu-precipitation kinetics in alpha-Fe from atomistic simulations: Vacancy-trapping effects and Cu-cluster mobility. *Physical Review B,* 76(21), 214102. https://doi.org/10.1103/PhysRevB.76.214102

[4] G. Bonny, D. Terentyev, L. Malerba, (2004). Structural stability and magnetic properties of metastable Fe-Cu alloys studied by ab initio calculations and molecular dynamics simulations. *Physical Review B*, 69(5), 054203. https://doi.org/10.1103/PhysRevB.69.054203

[5] M. Kaya, H. Çetin, B. Boyarbay, A. Gök, E. Ayyıldız, (2007). Temperature dependence of the current–voltage characteristics of Sn/PANI/p-Si/Al heterojunctions. *Journal of Physics: Condensed Matter*, 19(40), 406205. https://doi.org/10.1088/0953-8984/19/40/406205

[6] S. Liu, J. Jie, Z. Guo, S. Yue, T. Li, (2019). A comprehensive investigation on microstructure and magnetic properties of immiscible Cu-Fe alloys with variation of Fe content. *Materials Chemistry and Physics*, 238, 121909. https://doi.org/10.1016/j.matchemphys.2019.121909

[7] C. Zhang, C. Chen, Z. Guo, et al., (2021). Microstructure and properties of Cu-Fe alloys fabricated via powder metallurgy and rolling. *Materials and Manufacturing Processes*, 64(4).
https://doi.org/10.1080/00325899.2021.1890403

[8] Y. Ding, X. Xiao, D. Yuan, J. Chen, (2025). A study on the microstructure and properties of Cu-Fe-Mg-Ti alloys based on composition regulation. *Materials*, 18(6), 1325. https://doi.org/10.3390/ma18061325

[9] Y. Gao, H. Liu, Z. Chen, L. Zuo, J. Zhang, T. Zhang, (2026). Mechanism of liquid-liquid phase separation and crystal nucleation in Fe-Cu immiscible alloy doped with trace Zr. *Journal of Alloys and Compounds*, 1057, 186769. https://doi.org/10.1016/j.jallcom.2026.186769

[10] W. L. Wang, Y. H. Wu, L. H. Li, W. Zhai, X. M. Zhang, B. Wei, (2015). Liquid-liquid phase separation of freely falling undercooled ternary Fe-Cu-Sn alloy. *Scientific Reports*, 5, 16335.
https://doi.org/10.1038/srep16335

[11] T. T. T. Giap, K. H. Pham, (2025). Influence of composition on phase transition, crystallization, and glass transition temperatures of Fe1–xCux alloys (x = 0.2, 0.4, 0.5, 0.6, 0.8) studied via molecular dynamics simulations. *ACS Omega*, 10(31). https://doi.org/10.1021/acsomega.5c02498

[12] A. Caro, M. Caro, E. M. Lopasso, P. E. A. Turchi, D. Farkas, (2006). Thermodynamics of Fe-Cu alloys as described by a classic potential. *Journal of Nuclear Materials*, 349(3), 317–326.
https://doi.org/10.1016/j.jnucmat.2005.11.004

[13] A. Fantin, G. O. Lepore, M. Widom, S. Kasatikov, A. M. Manzoni, (2023). How atomic bonding plays the hardness behavior in the Al-Co-Cr-Cu-Fe-Ni high entropy family. *Small Science*, e2300225.
https://doi.org/10.1002/smsc.202300225

[14] D. N. Tran, L. V. Cao, S. Talu, (2022). Molecular dynamics simulation of Bulk Cu Material under Various Factors. *Applied Sciences*, 12(9), 4437. https://doi.org/10.3390/app12094437

[15] A. Caro, M. Caro, E. M. Lopasso, P. E. A. Turchi, D. Farkas, (2006). "Thermodynamics of Fe–Cu alloys as described by a classic potential." *Journal of Nuclear Materials*, 349(3), 317–326.
https://doi.org/10.1016/j.jnucmat.2005.11.004

[16] A. Fantin et al., (2023). How Atomic Bonding Plays the Hardness Behavior in the Al-Co-Cr-Cu-Fe-Ni HighEntropy Alloy. *Small Sci.*, 4, e2300225. https://doi.org/10.1002/smsc.202300225

[17] D. Reith, M. Stöhr, R. Podloucky, T. C. Kerscher, S. Müller, (2012). First-principles modeling of temperature and concentration-dependent solubility in the phase-separating alloy FexCu1-x. *Phys. Rev. B*, 86, 020201. https://doi.org/10.1103/PhysRevB.86.020201

[18] A. I. Dyachenko, V. E. Zakharov, (2016). Spatial equation for water waves. *JETP Letters*, 103(3), 181–184. https://doi.org/10.1134/S0021364016030048

[19] D. B. Miracle, (2004). A structural model for metallic glasses. *Nature Materials*, 3(10), 697–702. https://doi.org/10.1038/nmat1219

[20] D. Choudhuri, B. S. Majumdar, (2020). Structural changes during crystallization and vitrification of dilute FCC-based binary alloys. *Materialia*, 12, 100816. https://doi.org/10.1016/j.mtla.2020.100816

[21] C. Zhang, W. Peng, Y. Shao, M. Oleksandr, L. Lu, X. Zhang, (2024). Study on the melting and sintering behavior of Cu-Fe mixed nanoparticles based on molecular dynamics simulations. *Materials & Design*, 248, 113457. https://doi.org/10.1016/j.matdes.2024.113457

[22] H. Murdoch, A. Giri, D. Field, E. Hernández-Rivera, M. Guziewski, (2021). Magnetically altered phase stability in Fe-based alloys: Modeling and database development. *Calphad*, 75, 102360. https://doi.org/10.1016/j.calphad.2021.102360

[23] S. B. Luo, W. L. Wang, J. Chang, Z. C. Xia, B. Wei, (2014). A comparative study of dendritic growth within undercooled liquid pure Fe and Fe50Cu50 alloy. *Acta Materialia*, 69, 355-364. https://doi.org/10.1016/j.actamat.2013.12.009

[24] N. Duxin, N. Brun, C. Colliex, M. P. Pileni, (1998). Synthesis and magnetic properties of elongated Fe-Cu alloys. *Langmuir*, 14(8), 1984–1989. https://doi.org/10.1021/la9709094

[25] L. Chen, K. Nishida, K. Murakami, D. Chen, L. Liu, T. Kobayashi, Z. Li, N. Sekimura, (2019). A model to evaluate the hardening effect of solute clusters in Fe-based alloys. *Nuclear Instruments and Methods in Physics Research Section B: Beam Interactions with Materials and Atoms*, 455, 32-34. https://doi.org/10.1016/j.nimb.2019.06.022

[26] Q. L. Wang, J. Z. Zhao, (2010). A model describing the microstructure evolution in Fe-Cu alloys during thermal aging. *Materials Science and Engineering: A*, 528(1), 268-272. https://doi.org/10.1016/j.msea.2010.09.012

[27] R. Ali, B. Kamran, (2017). Identification of Crystal Structures in Atomistic Simulation by Predominant Common Neighborhood Analysis. *Computational Materials Science*, 126, 182–190. https://doi.org/10.1016/j.commatsci.2016.09.035

[28] U. Sarac, M. Kaya, M. C. Baykul, (2018). The influence of deposit composition controlled by changing the relative Fe ion concentration on properties of electroplated nanocrystalline Co-Fe-Cu ternary thin films. *Turkish Journal of Physics*, 42(2), 136-145. https://doi.org/10.3906/fiz-1706-6

[29] U. Sarac, M. Kaya, M. C. Baykul, (2016). Differences observed in the surface morphology and microstructure of Ni-Fe-Cu ternary thin films electrochemically deposited at low and high applied current densities. *Journal of Physics: Conference Series*, 766(1), 012025. https://doi.org/10.1088/1742-6596/766/1/012025

[30] S. Plimpton, (1995). Fast parallel algorithms for short-range molecular dynamics. *Journal of Computational Physics*, 117(1), 1-19. https://doi.org/10.1006/jcph.1995.1039

[31] M. S. Daw, M. I. Baskes, (1984). Embedded-Atom Method: Derivation and Application to Impurities, Surfaces, and Other Defects in Metals. *Physical Review B*, 29(12), 6443–6453. https://doi.org/10.1103/PhysRevB.29.6443

[32] D. R. Trinkle, (2025). Computing ternary liquid phase diagrams: Fe-Cu-Ni. *Physical Review Materials*, 9, 073801. https://doi.org/10.1103/c1zj-cg88

[33] T. Fang, L. Wang, C. X. Peng, Y. Qi, (2012). Liquid immiscibility in an Fe-Cu alloy by molecular dynamics simulation. *Journal of Physics: Condensed Matter*, 24(50), 505103. https://doi.org/10.1088/0953-8984/24/50/505103

[34] P. Hirel, (2015). Atomsk: A tool for manipulating and converting atomic data files. *Computer Physics Communications*, 197, 212–219. https://doi.org/10.1016/j.cpc.2015.07.012

[35] M. S. Daw, M. I. Baskes, (1983). Semiempirical, quantum mechanical calculation of hydrogen embrittlement in metals. *Physical Review Letters*, 50, 1285–1288. https://doi.org/10.1103/PhysRevLett.50.1285

[36] P. H. Hünenberger, (2005). Thermostat algorithms for molecular dynamics simulations. In: *Advanced Computer Simulation*. Advances in Polymer Science, vol. 173, pp. 105–149. https://doi.org/10.1007/b99427

[37] L. Verlet, (1967). Computer "experiments" on classical fluids. I. Thermodynamical properties of Lennard-Jones molecules. *Physical Review*, 159, 98–103. https://doi.org/10.1103/PhysRev.159.98

[38] L. Verlet, (1968). Computer "experiments" on classical fluids. II. Equilibrium correlation functions. *Physical Review*, 165, 201–214. https://doi.org/10.1103/PhysRev.165.201

[39] A. Stukowski, (2010). Visualization and analysis of atomistic simulation data with OVITO–the Open Visualization Tool. *Modelling and Simulation in Materials Science and Engineering*, 18(1), 015012. https://doi.org/10.1088/0965-0393/18/1/015012

[40] S. Nosé, (1984). A unified formulation of the constant temperature molecular dynamics methods. *The Journal of Chemical Physics*, 81(1), 511-519. https://doi.org/10.1063/1.447334

[41] D. B. Miracle, (2004). A structural model for metallic glasses. *Nature Materials*, 3, 697-702. https://doi.org/10.1038/nmat1219

[42] H. W. Sheng, W. K. Luo, F. M. Alamgir, J. M. Bai, E. Ma, (2006). Atomic packing and short-to-medium-range order in metallic glasses. *Nature*, 439, 419-425. https://doi.org/10.1038/nature04421

[43] T. Egami, (2011). Atomic level stresses. *Progress in Materials Science*, 56(6), 637-653. https://doi.org/10.1016/j.pmatsci.2011.01.004